IEEE Access
Multidisciplinary | Rapid Review | Open Access Journal

Received September 11, 2020, accepted September 26, 2020, date of publication September 30, 2020,
date of current version October 12, 2020.

Digital Object Identifier 10.1109/ACCESS.2020.3027851

Mobile Molecular Communication Through Multiple Measurements of the Concentration of Molecules

YUTAKA OKAIE AND TADASHI NAKANO, (Member, IEEE)
Institute for Datability Science, Osaka University, Suita 565-0871, Japan

Corresponding author: Yutaka Okaie (yokaie@fbs.osaka-u.ac.jp)

This work was supported by JSPS KAKENHI Grant Number JP20K19784.

ABSTRACT Multiple measurements of the concentration of molecules serve as a useful technique to enable bio-nanomachines to reliably extract information encoded in the concentration of molecules. In this paper, we develop mathematical models to examine the impact of multiple measurements of the concentration of molecules on the performance of mobile molecular communication taking into account the constrains associated with the systems. In this scenario, a mobile transmitter bio-nanomachine releases a pre-defined number of molecules and a mobile receiver bio-nanomachine receives information by measuring the concentration of these molecules on multiple occasions. Numerical results obtained using the models show that multiple measurements of the concentration of molecules serve as an effective means to improve mobile molecular communication performance.

INDEX TERMS Molecular communication, multiple measurements, demodulation, mobile molecular communication, bio-nanomachine.

I. INTRODUCTION

Molecular communication has emerged as an enabling technology for nano-scale communication between bio-nanomachines. In molecular communication, bio-nanomachines communicate with each other by propagating signal molecules in the environment [1]–[4]. Bio-nanomachines are of a nano-to-micrometer size dimension, are composed of biomaterials, and are capable of biochemical functionalities such as detecting a specific type of molecules, storing and releasing molecules, and converting chemical energy into mechanical motion. As molecular communication is energy efficient and compatible with biological environments, its application to medicine is anticipated [5].

In molecular communication, *multiple measurements* of the concentration of molecules provide a useful means for bio-nanomachines to reliably extract information encoded in the concentration of molecules [6]–[8]. In a scenario of this type, a transmitter bio-nanomachine releases a pre-defined number of molecules to transmit an information bit, while a receiver bio-nanomachine makes multiple measurements of the concentration of molecules, propagating in the environment to determine what information bit was transmitted. By measuring the concentration of molecules multiple times, a receiver bio-nanomachine can increase the measurement accuracy and decrease the error rate in receiving the transmitted bit.

The best strategy for bio-nanomachines to reliably extract information encoded in the concentration of molecules in the environment is for them to continuously measure the concentration of molecules. However, the number of measurements that bio-nanomachines can perform may be limited for several reasons. First, successive measurements need to be made with a sufficient time interval in between to ensure that the measurements are statistically independent from each other, thus enabling the concentration of molecules to be obtained accurately through averaging [9], [10]. Second, bio-nanomachine receptors that measure the concentration of molecules in the environment behave stochastically; they bind to and unbind from molecules probabilistically [11], they perform random walks over the surface of or within a bio-nanomachine [12], and they are internalized and recycled upon binding to molecules [13]. Due to these receptor behaviors, it may not be possible for bio-nanomachines to

The associate editor coordinating the review of this manuscript and approving it for publication was Xiaofan He.

This work is licensed under a Creative Commons Attribution 4.0 License. For more information, see https://creativecommons.org/licenses/by/4.0/

measure the concentration of molecules continuously. Third, bio-nanomachines may use oscillatory biochemical reactions to measure the concentration of molecules in the environment [14]; the receptors' sensitivity may oscillate [15] or the bio-nanomachines' internal state may oscillate [16]. Bio-nanomachines may make measurements at the frequency of such oscillatory reactions.

The contribution of this paper is to examine the impact of multiple measurements of the concentration of molecules on mobile molecular communication performance. Mobile molecular communication is characterized by the fact that both the transmitter and receiver bio-nanomachines are mobile [17]. In mobile molecular communication, transmitter and receiver bio-nanomachines change their spatial positions stochastically due to intrinsic or extrinsic noise. No previous work has investigated the impact of multiple measurements on mobile molecular communication performance. In this paper, we first develop a mathematical model of mobile molecular communication wherein a mobile transmitter releases molecules to transmit bits of information, and a mobile receiver makes multiple measurements to receive the transmitted bits. We then use the model to conduct numerical experiments and examine the impact of key model parameters on the rate and accuracy of information transfer.

The remainder of this paper is organized as follows. Section II describes related work, including modulation techniques for molecular communication, and mobile molecular communication, and multiple measurements of the concentration of molecules. Section III provides an overview of the mobile molecular communication system considered in this paper. The mathematical model for the considered system is then developed in Section IV and numerical results obtained with the model are presented in Section V. Finally, Section VI discusses future work to conclude the paper.

II. RELATED WORK

A. CONCENTRATION SHIFT KEYING

In this paper, we consider molecular communication based on concentration shift keying (CSK). CSK is a technique that modulates the concentration of molecules to represent information [2], [18]–[23]. In CSK, a transmitter bio-nanomachine releases molecules in a pulse or a waveform manner. Molecules released by the transmitter bio-nanomachine propagate via diffusion in the environment and decay or degrade over time. By comparing the observed concentration against a pre-specified threshold, a receiver bio-nanomachine extracts information from the concentration of molecules that it observes. CSK is commonly employed in biological systems where biological cells respond to the high concentration of molecules and profiles as one of the simplest techniques for engineered molecular communication. CSK is also employed in tabletop molecular communication [24].

In CSK-based molecular communication, inter-symbol interference (ISI) is a major issue that needs to be resolved. Due to the heavy-tail nature of molecular diffusion, molecules that a transmitter bio-nanomachine transmits serve as noise in future transmissions of molecules. To mitigate the ISI effect, several techniques have been proposed, such as using the ISI-aware channel code [25] and using adaptive thresholds in demodulation [26]. In this paper, we mitigate the effect of ISI in a relatively simple manner by determining the receiver bio-nanomachine's threshold after taking into account the concentrations of molecules released in previous transmissions.

B. MOBILE MOLECULAR COMMUNICATION

Mobile molecular communication is an emerging area in molecular communication that is, as its name suggests, characterized by mobile transmitter and receiver bio-nanomachines [17]. Here, transmitter and receiver bio-nanomachines may move due to intrinsic or extrinsic noise, and change their spatial positions stochastically. This type of random mobility may disturb the desired behavior or operations of bio-nanomachines [27]–[37] or can improve the performance of communication under specific settings [38]–[40]. Transmitter and receiver bio-nanomachines may also move directionally, such as is seen in chemotactic cells [41], and directional motion of bio-nanomachines may be useful in developing specific molecular communication mechanisms [42]–[46] or employed in developing practical applications [5], [47]–[53].

C. MULTIPLE MEASUREMENTS

The concentration of molecules in the environment fluctuates due to thermal noise. To determine the fluctuating concentration of molecules, biological cells measure the concentration of molecules multiple times during a time interval and average the measurements made in the interval [9], [10]. To ensure that a measurement is statistically independent from its previous measurement, biological cells need to wait for a period of $V^{\frac{2}{3}}/D$ where V is the volume of the cell and D is the diffusion coefficient of molecules, indicating time required for a molecule to diffuse out of the volume space.

In the molecular communication system proposed in [6], [7], a micro-scale receiver (e.g., an engineered cell and an electrical device) acts as a base station which gathers information that nano-transmitters transmitted through molecules. The micro-scale receiver measures the concentration of molecules over time to determine what information was transmitted. It is shown that, through multiple measurements and statistical methods, the micro-scale receiver can more accurately determine information transmitted. Unlike these previous works, this paper examines the impact of the number of measurements in mobile molecular communication.

III. SYSTEM OVERVIEW

Figure 1 depicts the molecular communication system considered in this paper. Here, a mobile transmitter bio-nanomachine (Tx) communicates with a mobile receiver bio-nanomachine (Rx) by propagating molecules in

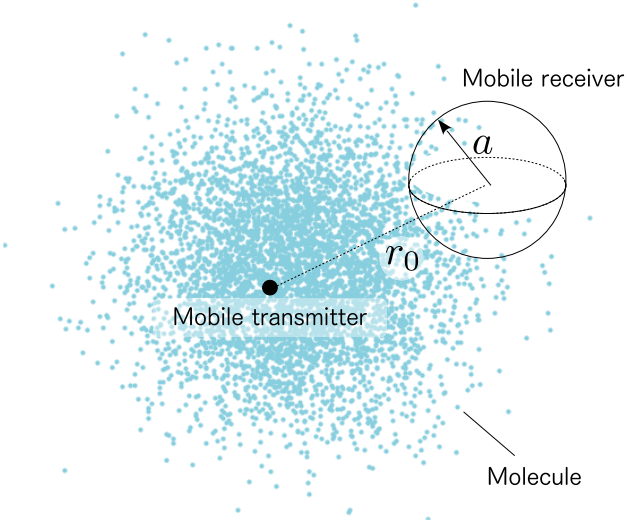

FIGURE 1. System overview. Transmitter is a point source, and receiver is a sphere of radius a. Tx and Rx are initially distance r_0 apart.

a three-dimensional unbounded environment. Tx and Rx are mobile and move randomly in the environment. Naturally occurring and genetically engineered cells are examples of Tx and Rx [4]. The environment is aqueous, such as the in-body environment in which molecules may propagate.

In this system, Tx and Rx are perfectly synchronized throughout their molecular communication. Time is slotted by a fixed length, and Tx transmits a symbol (0 or 1, see below) to Rx in each time slot. In the following, we explain the three key phases of molecular communication: signal modulation, signal propagation, and signal demodulation.

Signal modulation: Tx uses the Binary Concentration Shift Keying (BCSK), one of the simplest modulation techniques for molecular communication [20], to transmit a symbol in each time slot. At the beginning of each time slot, Tx releases a pre-defined number of molecules to transmit symbol '0' or another pre-defined number of molecules to transmit symbol '1'.

Signal propagation: Molecules transmitted by Tx propagate via free diffusion in the three-dimensional unbounded environment. Also, molecules transmitted by Tx react with molecules in the environment and degrade over time. There is no flow or advection in the environment that may disturb the diffusion of molecules.

Signal demodulation: Rx measures the concentration of molecules at its location. This concentration may be subject to inter-symbol interference (ISI) due to residual molecules released in previous time slots. The concentration of molecules at Rx's location is also subject to diffusion noise and fluctuates stochastically [54]. Rx makes multiple measurements of the concentration of molecules in each time slot; it receives '1' from a slot when the concentration of molecules in any measurement in the slot exceeds a threshold, and it receives '0' otherwise (i.e., when all the measurements are below the threshold). This simple modulation algorithm can be easily designed using concentration-dependent chemical reactions that occur when the concentration of molecules exceeds a threshold value.

IV. MATHEMATICAL MODELS

In this section, we develop mathematical models to describe the mobile molecular communication system outlined in Section III.

A. BIO-NANOMACHINE MOBILITY

When the transmitter bio-nanomachine Tx, initially located at the origin of the coordinate system, performs a random walk in one-dimensional space, the probability distribution of Tx's location, x, at time t is given by

$$p(x;t) = \frac{1}{\sqrt{4\pi D_{\mathrm{T}}\, t}} \exp\left(-\frac{x^2}{4\, D_{\mathrm{T}}\, t}\right), \tag{1}$$

where D_{T} represents the diffusion coefficient of Tx [55]. Similarly, the receiver bio-nanomachine Rx, initially located at distance x_0 from Tx, performs a random walk with diffusion coefficient D_{R}, the probability distribution of Rx's location, x, at time t is given by

$$q(x;x_0,t) = \frac{1}{\sqrt{4\pi D_{\mathrm{R}}\, t}} \exp\left(-\frac{(x-x_0)^2}{4\, D_{\mathrm{R}}\, t}\right). \tag{2}$$

Using (1) and (2), we can write the probability distribution of the distance between Tx and Rx as

$$\begin{aligned} R(d_x;x_0,t) &= \int_{-\infty}^{+\infty} p(x;t)\, q(x+d_x;x_0,t)\mathrm{d}x \\ &= \frac{1}{\sqrt{4\pi D_{\mathrm{T,R}}\, t}} \exp\left(-\frac{(d_x-x_0)^2}{4\, D_{\mathrm{T,R}}\, t}\right) \end{aligned} \tag{3}$$

where $D_{\mathrm{T,R}}$ is the sum of the two diffusion coefficients D_{T} and D_{R} $\left(D_{\mathrm{T,R}} = D_{\mathrm{T}} + D_{\mathrm{R}}\right)$ [56]. From (3), the variance of d_x is $2\, D_{\mathrm{T,R}}\, t$, meaning that the root mean square, and therefore the distance between Tx and Rx, increases in proportion to $\sqrt{D_{\mathrm{T,R}}\, t}$.

When Tx and Rx perform random walk in three-dimensional space, we multiply (3) for the x, y, and z coordinates, and obtain the probability distribution of the distance between Tx and Rx as

$$R(\vec{r};\vec{r}_0,t) = \frac{1}{\left(4\pi D_{\mathrm{T,R}}\, t\right)^{3/2}} \exp\left(-\frac{|\vec{r}-\vec{r}_0|^2}{4\, D_{\mathrm{T,R}}\, t}\right), \tag{4}$$

where $\vec{r} = \left(d_x, d_y, d_z\right)$ and $\vec{r}_0 = (x_0, y_0, z_0)$ [57].

B. SIGNAL MODULATION

In the molecular communication considered in this paper, time is slotted by constant length, T, and Tx releases a pre-specified number of molecules A_b for a binary symbol $b \in \mathbb{B} = \{0, 1\}$ at the beginning of each time slot. The concentration of molecules due to the molecules Tx transmits at time t is thus expressed as

$$f(t) = \sum_{j=1}^{\lfloor \frac{t}{T} \rfloor} A_{b_j} \delta(t - jT), \tag{5}$$

where b_j is the symbol transmitted at the j-th slot and $\delta(\cdot)$ is the Dirac delta function.

C. SIGNAL PROPAGATION

Assume that in one-dimensional space Tx and Rx are initially located at distance d_x from each other. Tx releases A_b molecules to transmit symbol $b \in \mathbb{B} = \{0, 1\}$, and the released propagate with diffusion coefficient D_{M} in the environment and degrade with degradation rate constant, κ. Rx, on the other hand, performs a random walk with diffusion coefficient D_{R}, such that the concentration of molecules at Rx's location after time t is given by

$$g(t; d_x, b) = \frac{A_b}{\sqrt{4\pi D_{\mathrm{M,R}}\, t}} \exp\left(-\frac{d_x^2}{4\, D_{\mathrm{M,R}}\, t} - \kappa t\right), \quad (6)$$

where $D_{\mathrm{M,R}}$ is the sum of the two diffusion coefficients D_{M} and D_{R} $\left(D_{\mathrm{M,R}} = D_{\mathrm{M}} + D_{\mathrm{R}}\right)$.

We further assume that Tx is mobile and performs a random walk before it releases molecules. Tx and Rx are initially located at distance x_0 away from each other, and before Tx releases molecules, both Tx and Rx perform random walks for time duration s. Under this assumption, the concentration of molecules at Rx's location becomes

$$\begin{aligned} h(t, s; b) &= \int_{-\infty}^{+\infty} g(t; d_x, b) \times R(d_x; x_0, s)\mathrm{d}d_x \\ &= \frac{A_b}{\sqrt{4\pi\left(D_{\mathrm{M,R}}\, t + D_{\mathrm{T,R}}\, s\right)}} \\ &\quad \times \exp\left(-\frac{x_0^2}{4\left(D_{\mathrm{M,R}}\, t + D_{\mathrm{T,R}}\, s\right)} - \kappa t\right). \end{aligned} \quad (7)$$

Note that, in this equation, t is the time duration during which molecules propagate, and s is the time duration during which both Tx and Rx perform their random walks before Tx releases molecules. By using the concept of effective diffusion coefficients, mobile molecular communication is transformed into a static communication where molecules diffuse with the effective diffusion coefficient and Rx is at a fixed location [58], [59].

When the environment is three-dimensional, we can write the concentration of molecules at Rx's location as

$$\begin{aligned} h(t, s; b) &= \frac{A_b}{\left(4\pi\left(D_{\mathrm{M,R}}\, t + D_{\mathrm{T,R}}\, s\right)\right)^{3/2}} \\ &\quad \times \exp\left(-\frac{|\vec{r}_0|^2}{4\left(D_{\mathrm{M,R}}\, t + D_{\mathrm{T,R}}\, s\right)} - \kappa t\right), \end{aligned} \quad (8)$$

where $|\vec{r}_0|^2 = x_0^2 + y_0^2 + z_0^2$.

Figure 2 compares the concentration of molecules obtained from (8) and that from Monte Carlo simulations. In this figure, Mote Carlo simulations are performed as follows. At time $t = 0$, Tx is placed at the origin, and Rx at $(r_0, 0, 0)$ in 3-dimensional space. Tx releases the number A_b of molecules at $t = 0$ (i.e., $s = 0$) in a pulse. Time is discretized by Δt. At each time step, Rx migrates by $\pm\sqrt{2\, D_{\mathrm{R}}\, \Delta t}$ along each coordinate in the 3-dimensional space. At each time step, the distance between the origin and Rx (mobile), represented by $r(t)$, is updated and the concentration of molecules at Rx's location at time t is obtained from the following equation:

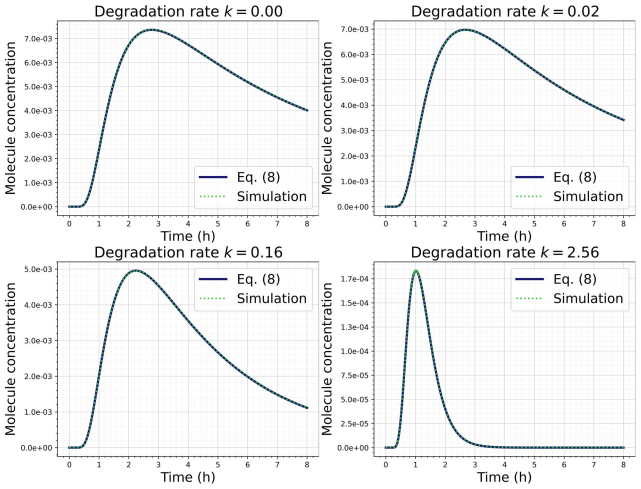

FIGURE 2. Concentration of molecules as a function of time according to (8) and from Monte Carlo simulations.

$$\frac{A_b}{(4\, D_{\mathrm{M}}\, t)^{3/2}} \exp\left(-\frac{r^2(t)}{4\, D_{\mathrm{M}}\, t} - \kappa t\right). \quad (9)$$

In this figure, we use the following parameter values: $A_b = 100,000$, $D_{\mathrm{M}} = 300\ \mu\mathrm{m}^2/\mathrm{h}$, $D_{\mathrm{R}} = 300\ \mu\mathrm{m}^2/\mathrm{h}$, $r_0 = 100\ \mu\mathrm{m}$, the volume of Rx is $1.0\ \mu\mathrm{m}^3$, and $\Delta t = 0.02$ h. The figure plots the mean concentration of molecules computed from $1,000,000$ realizations. As shown in the figure, the concentration of molecules obtained from (8) coincides with that from the simulations.

D. SIGNAL DEMODULATION

The concentration of molecules at Rx's location is given by the sum of the concentrations of molecules released in all previous time slots as well as that from the current slot. Given a transmitted symbol sequence $(b_1, b_2, \cdots, b_k)$, the concentration of molecules at Rx's location after time t has passed since the beginning of the k-th slot is given by

$$\begin{aligned} h^{(k)}(t; b_1, b_2, \cdots, b_k) &= h(t, (k-1)T; b_k) \\ &\quad + \sum_{i=1}^{k-1} h(t + (k-i)T, (i-1)T; b_i). \end{aligned} \quad (10)$$

The second term on the right-hand side of (10) represents the concentration of residual molecules that interfere with the transmission of the signal for the current, k-th slot; this is referred to as the inter-symbol interference (ISI). Since the previously transmitted symbol sequence is unknown to Rx, Rx estimates the residual molecule concentration (ISI) by assuming that Tx transmits 0 and 1 equiprobably in all the previous slots. In this case, the estimated concentration of molecules at Rx's location at time t in the k-th slot, when

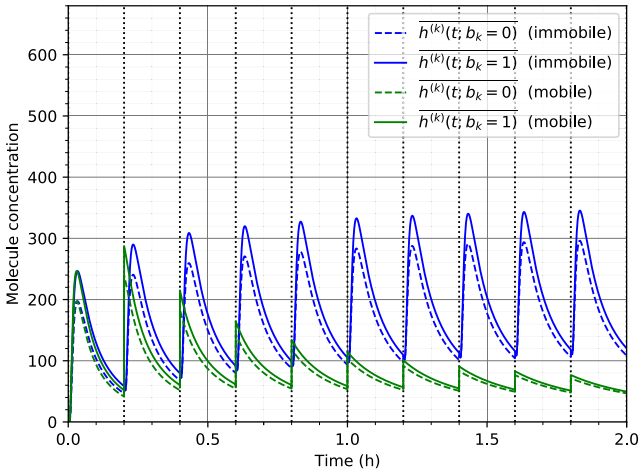

FIGURE 3. Concentration of molecules when bio-nanomachines are mobile and immobile: $D_T = D_R = 5000$ when mobile, and 0 when immobile. $D_M = 50000$, $r_0 = 100$, $T = 0.2$, $A_1 = 100000$, $A_0 = 80000$, and $\kappa = 0.01$.

the k-th bit is b_k, is

$$\overline{h^{(k)}(t;b_k)} = \frac{1}{2^{k-1}} \sum_{(b_1,\cdots,b_{k-1})\in\mathbb{B}^{k-1}} h^{(k)}(t;b_1,b_2,\cdots,b_k). \tag{11}$$

Figure 3 plots the concentrations of molecules at Rx's location given by (11) when bio-nanomachines are mobile ($D_{M,R} > 0$) and immobile ($D_{M,R} = 0$). For each time slot, a single symbol is transmitted for 1 bit of information. In our model, Rx observes the concentrations of molecules at multiple occasions in Figure 3. When bio-nanomachines are immobile, the *peak* concentration of molecules at Rx's location at a certain time slot increases over time due to the ISI effect. However, the increase in peak concentration of molecules becomes smaller and smaller with time, since molecules transmitted by Tx will disperse and decay to produce no significant effect after a sufficiently long time has elapsed. When bio-nanomachines are mobile, the peak concentrations of molecules at Rx's location comes earlier and becomes smaller than the immobile case in the 2nd and subsequent slots. This occurs for several reasons. First, bio-nanomachine mobility increases the effective diffusion coefficient of molecules; this contributes the earlier arrival of peak in the concentration of molecules at Rx's location. Second, since Tx and Rx move, the distance between Tx and Rx (or the root mean square distance) increases as time progresses; this contributes to the decrease in the concentration of molecules at Rx's location.

The concentration of molecules Rx detects is subject to diffusion noise, and is known to follow a normal distribution with the mean and variance equal to the concentration of molecules at Rx's location, i.e., $\mathcal{N}\left(h^{(k)}(t^*;b_k), h^{(k)}(t^*;b_k)\right)$ where t^* is the time at which Rx makes the measurement [54]. The probability distribution of the mean concentration of molecules with diffusion noise measured at time t in the k-th slot is

$$f^{(k)}_{b_k}(c;t) = \frac{1}{\sqrt{2\pi\ \overline{h^{(k)}(t;b_k)}}} \exp\left(-\frac{\left(c-\overline{h^{(k)}(t;b_k)}\right)^2}{2\ \overline{h^{(k)}(t;b_k)}}\right). \tag{12}$$

In the molecular communication considered in this paper, Rx measures the concentration of molecules on multiple occasions at times $t \in \mathcal{T}^{(k)}_m = \left\{t^{(k)}_1, t^{(k)}_2, \cdots, t^{(k)}_m\right\}$ in the k-th slot, where m is the number of measurements. Here, the measurement time interval may be modeled by an exponential distribution with a parameter λ that represents the average number of measurements per unit time. λ may vary depending on the underlying biochemical processes enabling multiple measurements.

Rx measures the concentration of molecules multiple times in each time slot; it receives '1' from a slot when the concentration of molecules in any measurement in the slot exceeds a pre-defined concentration threshold ω, and it receives '0' otherwise (i.e., when all the measurements are below the threshold). This is translated to the following: Rx chooses the *maximum* concentration from the multiple measurements and compares the maximum concentration against ω to receive '1' or '0'. The cumulative probability function of the maximum concentration of molecules that Rx detects, when a symbol b_k is transmitted in the k-th slot, is

$$\begin{aligned} G^{(k)}_{b_k}(c;\mathcal{T}^{(k)}_m) &= \Pr\left[\max_{i\in\{1,\cdots,m\}} C^{(k)}_i < c \;\middle|\; B_k = b_k\right] \\ &= \Pr\left[C^{(k)}_1 < c, \cdots, C^{(k)}_m < c \;\middle|\; B_k = b_k\right] \\ &= \prod_{i\in\{1,\cdots,m\}} \int_{-\infty}^{c} f^{(k)}_{b_k}(c';t^{(k)}_i)\mathrm{d}c', \end{aligned} \tag{13}$$

where B_k and $C^{(k)}_i$ are random variables for the transmitted symbol and i-th measured molecule concentration in k-th slot. In our model, we assume that the transmitted symbol is chosen equiprobably, and define the error rate as

$$\begin{aligned} e(\omega) &= \frac{1}{2}\left\{\mathrm{P}_{Y_k|B_k}(1|0) + \mathrm{P}_{Y_k|B_k}(0|1)\right\} \\ &= \frac{1}{2}\left\{1 - G^{(k)}_0(\omega;\mathcal{T}^{(k)}_m) + G^{(k)}_1(\omega;\mathcal{T}^{(k)}_m)\right\}, \end{aligned} \tag{14}$$

where Y_k is the symbol Rx received in the k-th slot. Rx uses the threshold ω^* that minimizes the error rate $e(\omega)$ given above.

In the case where Rx makes a single measurement ($m = 1$), the threshold ω for the first slot ($k = 1$), or that for any slot when the time slot length T is sufficiently long and there is no ISI, becomes the following. In this case, the ratio of the two concentrations of molecules that Rx detects for symbols '0' and '1' is always equal to the ratio of the numbers of molecules Tx releases for symbols '0' and '1' (i.e., A_0 and A_1). Let α and β ($0 < \alpha < \beta$) be the concentrations of molecules that Rx detects, in the absence of diffusion

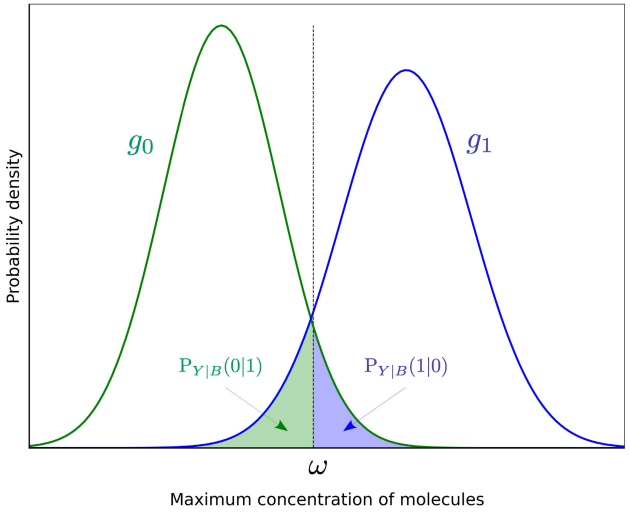

FIGURE 4. Determination of the threshold, ω.

noise, for symbols '0' and '1', respectively. The molecule concentrations in the presence of diffusion noise follow the normal distributions $\mathcal{N}(\alpha, \alpha)$ and $\mathcal{N}(\beta, \beta)$, and now we let the corresponding probability distribution functions be g_0 and g_1, respectively. We determine the threshold concentration ω^* from the first derivative test of (14):

$$\begin{aligned}\left.\frac{\partial e(\omega)}{\partial \omega}\right|_{\omega=\omega^*} &= \left.\frac{\partial}{\partial \omega}\left\{\int_{-\infty}^{\omega} g_1(c)\mathrm{d}c + \int_{\omega}^{+\infty} g_0(c)\mathrm{d}c\right\}\right|_{\omega=\omega^*} \\ &= g_1(\omega^*) - g_0(\omega^*) \\ &= \frac{1}{\sqrt{2\pi\beta}} \exp\left(-\frac{(\omega^*-\beta)^2}{2\beta}\right) \\ &\quad - \frac{1}{\sqrt{2\pi\alpha}} \exp\left(-\frac{(\omega^*-\alpha)^2}{2\alpha}\right) \\ &= 0. \end{aligned} \tag{15}$$

Note that the threshold ω^* is determined at the intersection of the curves for g_0 and g_1 (see Figure 4). The error rate for receiving a '0' when '1' is transmitted, i.e., $\mathrm{P}_{Y|B}(0|1)$, is shown as the green area, while that of receiving a '1' when a '0' is transmitted, i.e., $\mathrm{P}_{Y|B}(1|0)$, is shown as the blue area.

By solving (15), we have

$$\omega^* = \sqrt{\frac{\alpha\beta\left\{\log\left(\beta/\alpha\right) + \beta - \alpha\right\}}{\beta - \alpha}}, \tag{16}$$

and the corresponding error rate is given by

$$e(\omega^*) = \frac{1}{4}\left\{2 - \mathrm{erf}\,\frac{\omega^*-\alpha}{\sqrt{2\alpha}} + \mathrm{erf}\,\frac{\omega^*-\beta}{\sqrt{2\beta}}\right\}. \tag{17}$$

Figure 5 plots the error rate as a function of β. As shown in the figure, the error rate decreases as β increases for all five ratios of $A_0/A_1 = 0.1, 0.4, 0.6, 0.8$ and 0.9, meaning that Rx should make a measurement when the concentration of molecules reaches its peak. Since the concentration of

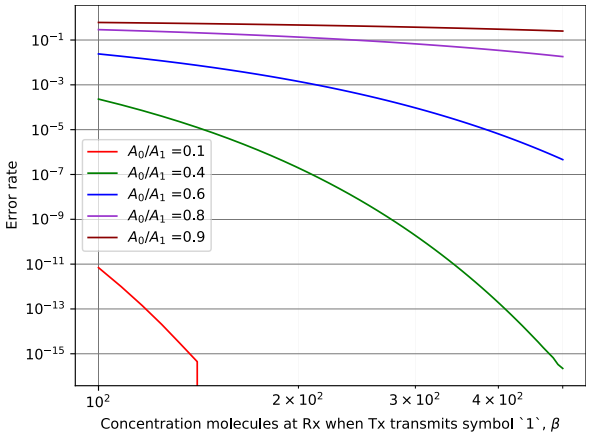

FIGURE 5. Error rate as a function of β.

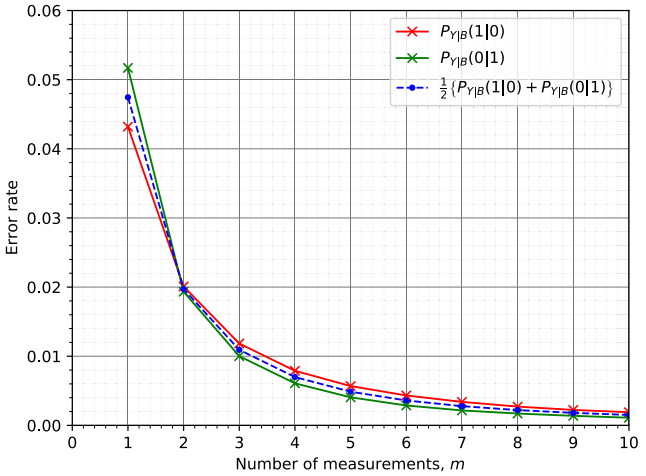

FIGURE 6. Error rates when the number of measurements, m, is varied.

molecules reaches its peak at

$$\begin{aligned} t_{\mathrm{peak}} &= \max_{0<t^*}\left\{\left.\frac{\mathrm{d}\,h(t;b)}{\mathrm{d}t}\right|_{t=t^*} = 0\right\} \\ &= \begin{cases} \dfrac{\sqrt{9D^2+4\kappa r_0^2 D}-3D}{4\kappa D} & (\kappa > 0), \\ \dfrac{r_0^2}{6D} & (\kappa = 0). \end{cases} \end{aligned} \tag{18}$$

the error rate is minimized when Rx makes a measurement at $t = t_{\mathrm{peak}}$, which is when the concentrations of molecules at Rx's location are $\alpha = h(t_{\mathrm{peak}}, 0; 0)$ and $\beta = h(t_{\mathrm{peak}}, 0; 1)$.

Figure 6 plots error rates as a function of the number of measurements, m, under the same conditions applied in Figure 5. For simplicity, Rx measures the same concentration of molecules through multiple measurements: $\alpha = 200$ for symbol '0' and $\beta = 250$ for symbol '1'. The figure show that, as m increases, both $\mathrm{P}_{Y|B}(1|0)$ and $\mathrm{P}_{Y|B}(0|1)$ decrease and thus the average error rate $\frac{1}{2}\left\{\mathrm{P}_{Y|B}(1|0) + \mathrm{P}_{Y|B}(0|1)\right\}$ also decreases, demonstrating the advantage of multiple measurements. It also shows that $\mathrm{P}_{Y|B}(0|1)$ is larger than

$P_{Y|B}(1|0)$ for $m = 1$. This is because the variance of the concentration of molecules for transmission of '1' is larger than that for transmission of '0'. It also shows that $P_{Y|B}(0|1)$ is smaller than $P_{Y|B}(1|0)$ for $m \geq 2$. This is because '1' is received when at least one measurement exceeds the threshold concentration; transmission of '1' is more error-resilient than that of '0'.

V. PERFORMANCE EVALUATION

A. CONFIGURATIONS

In numerical experiments, we evaluate the performance of the molecular communication using the achievable rate of the symbol transmission at the k-th slot

$$\max_{\Pr[B_k=b_k]\in[0,1]} \sum_{(b_k,c_k)\in\mathbb{B}^2} \Pr[B_k = b_k, C_k = c_k] \times \log \frac{\Pr[B_k = b_k, C_k = c_k]}{\Pr[B_k = b_k]\Pr[C_k = c_k]}. \quad (19)$$

For simplicity, Rx measures the concentration of molecules multiple times in each time slot at a regular time interval τ. The measurement times in the k-th slot are $\mathcal{T}_m^{(k)} = \{j\tau \mid j = 0, 1, \cdots, m-1\}$, where $m = \lfloor T/\tau \rfloor + 1$.

B. PARAMETER VALUES

In numerical experiments, we use the following parameter values: $a = 5$ μm, $D_{\mathrm{M,R}} = 50,000$ μm^2/h, $D_{T,R} = 10,000$ μm^2/h, $r_0 = 100$ μm, $A_1 = 100,000$ molecules, $A_0 = 80,000$ molecules, $\kappa = 0.01$ /h, $k = 15$ slot, and $T = 0.2$ h. The key parameter m is varied with $m = 10, 50, 100, 500, 1000$, and thus $\tau = \frac{T}{m}$ becomes $\tau = 0.02, 0.004, 0.002, 0.0004, 0.0002$ h, respectively. Note that we choose these values for illustrative purposes. Determining appropriate parameter values requires determining implementation details of molecular communication and experimentally identifying parameter values. We leave such implementation and experiments for future work.

C. NUMERICAL RESULTS

In numerical experiments, we examine the impact of the number m of measurements on the achievable rate in the k-th symbol transmission defined by (19). In all figures in this section, we show the achievable rate when Rx measures the concentration of molecules at a regular time interval of τ in the k-th slot. As will be shown in the figures, the achievable rate always increases with m; however, the effectiveness of increasing m depends significantly on parameter values used.

In the following, we show the impact of key model parameters on the achievable rate when multiple measurements are employed. Figure 7 shows the achievable rates when the number k of slots is varied between 1 and 20 for different values of m. As shown in the figure, the achievable rates decrease monotonously as k increases; this is because the distance between Tx and Rx in the k-th slot increases with time (i.e., with k), which significantly decreases the achievable rates. The decrease in achievable rate is also due to the interference between the symbol transmission in the current k-th slot and previous symbol transmissions (i.e., the ISI effect).

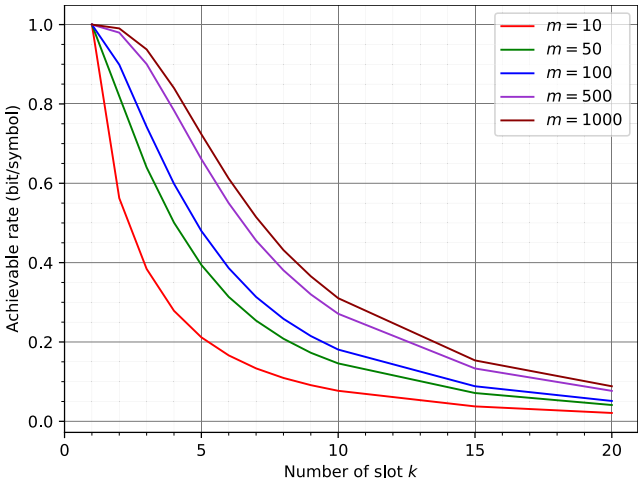

FIGURE 7. Impact of the number of slots k.

Figure 8 shows the achievable rates when the degradation rate κ of molecules is varied between 0 and 40 /h for different values of m. When κ increases from 0.01 to 10 /h, the achievable rates increase. This is because an increase in κ in this range mitigates the ISI effect. The figure also shows that a further increase in κ (> 10) negatively impacts the achievable rates. This is because, when the value of κ is too large, the concentration of molecules that the receiver detects decreases.

Figure 9 shows the achievable rates when the time slot length T is varied between 0.05 and 2 h for different values of m ($m = 50T, 250T, 500T, 2500T, 5000T$). Note that Rx makes measurements at a constant time interval of τ and thus, the number m of measurements increases with T in this figure. When T increases, the achievable rates decrease. In general, increasing T has both positive and negative effects on the achievable rate; the positive impact is the reduction of the ISI effect, whereas the negative effect is an increase in the distance between Tx and Rx due to mobility. The result captures that the negative impact becomes more significant under the parameter values used.

Figure 10 shows the achievable rates when the initial Tx-to-Rx distance r_0 is varied between 5 and 500 μm for different values of m. The achievable rates decrease with r_0 simply because the concentration of molecules Rx detects decreases as r_0 increases.

Figure 11 shows the achievable rates when the effective diffusion coefficient $D_{\mathrm{M,R}}$ is varied between 5000 and 100,000 μm^2/h for different values of m, where we assume typical protein molecules for the value of diffusion coefficient. The figure shows that, when $D_{\mathrm{M,R}}$ increases, the achievable rate increases. This is because, when $D_{\mathrm{M,R}}$ is larger, molecules released by Tx diffuse more quickly and more molecules reach Rx before they degrade. As a result,

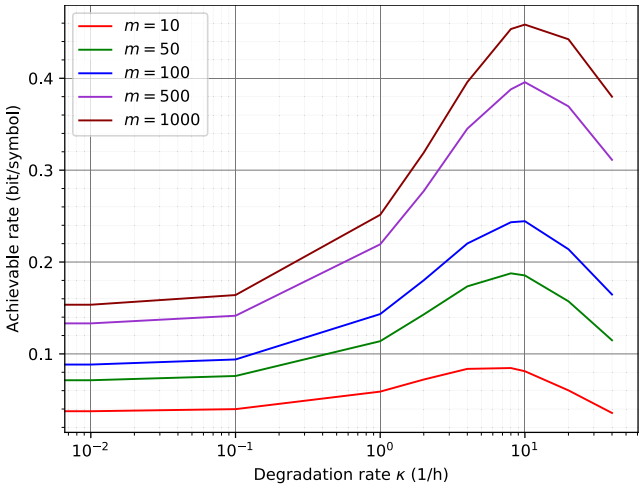

FIGURE 8. Impact of degradation rate κ.

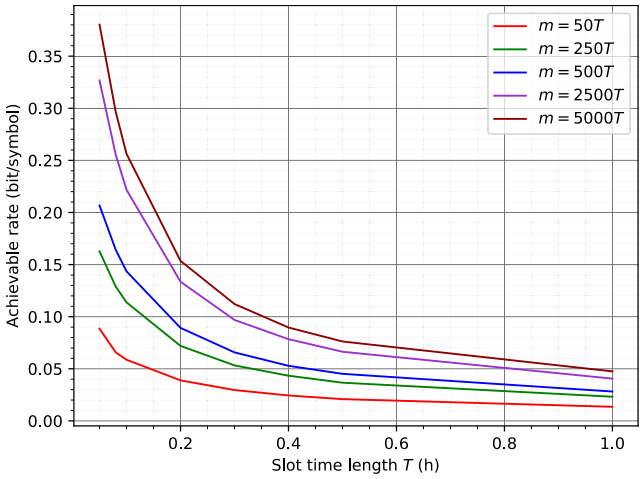

FIGURE 9. Impact of time slot length T.

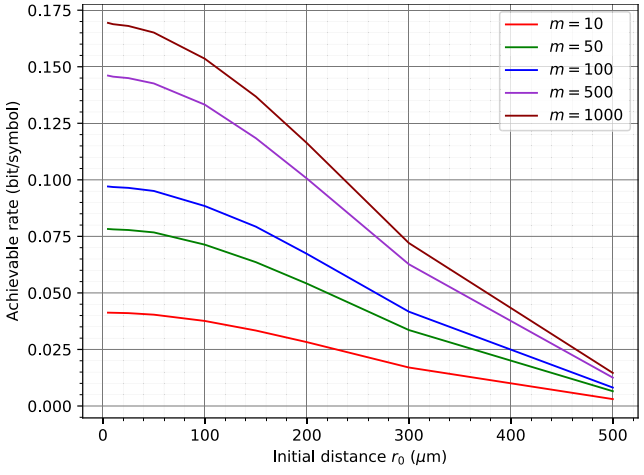

FIGURE 10. Impact of initial distance between Tx and Rx, r_0.

Rx measures a higher concentration of molecules, and this increases the achievable rate.

Figure 12 shows the achievable rates when the effective diffusion coefficient $D_{\mathrm{T,R}}$ is varied between 500 and

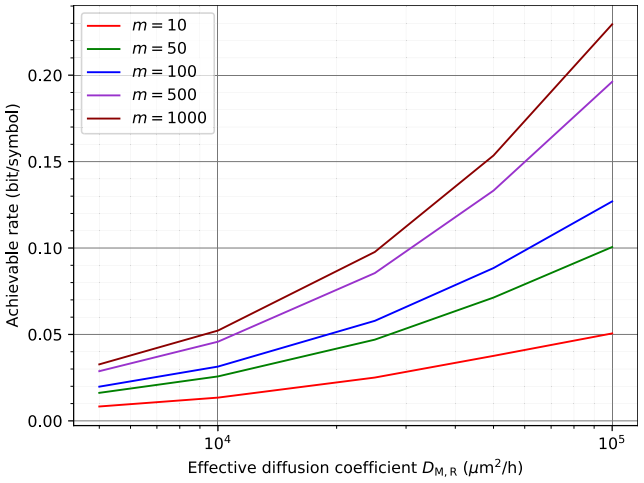

FIGURE 11. Impact of effective diffusion coefficient $D_{\mathrm{M,R}}$.

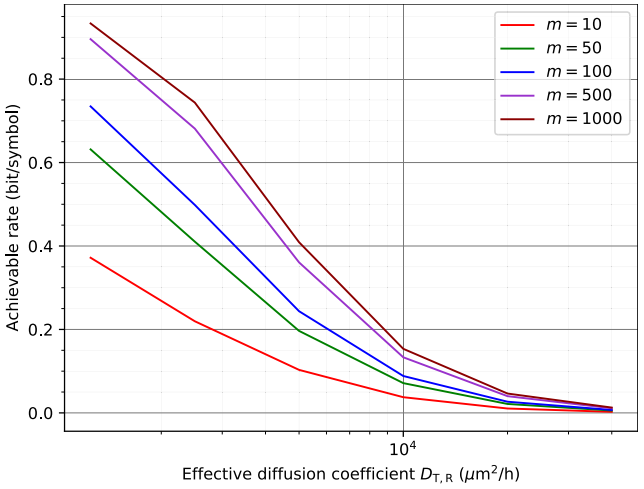

FIGURE 12. Impact of effective diffusion coefficient $D_{\mathrm{T,R}}$.

8000 μm^2/h for different values of m. The achievable rates decrease as $D_{\mathrm{T,R}}$ increases. This is because the Tx-to-Rx distance increases more rapidly with a larger value of $D_{\mathrm{T,R}}$ and thus this decreases the achievable rates.

Figure 13 shows the achievable rates when the ratio A_0/A_1 is varied between 0.5 and 0.9 for different values of m while A_1 is fixed to 100, 000. When the ratio increases, the achievable rates decrease given that Rx can determine more easily what symbol is transmitted when the ratio is larger or when the difference between the numbers of molecules released by Tx for symbols '0' and '1' is larger.

All numerical results presented in this section (Figures 7 through 13) show that the achievable rate increases with m for a given parameter value, demonstrating the effectiveness of multiple measurements in molecular communication. In Figure 7, for instance, the achievable rate for $k = 10$ increases from 0.27 to 0.31 when m is increased from 500 to 1000; and the achievable rate for $k = 15$ increases from 0.13 to 0.15 when m is increased from 500 to 1000. The numerical results also show that multiple measurements serve

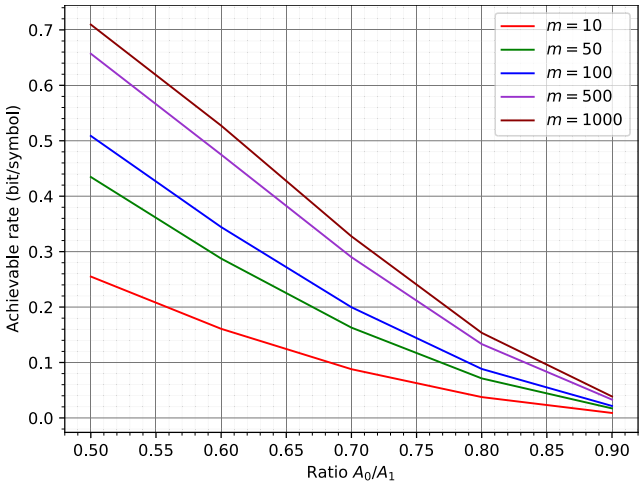

FIGURE 13. Impact of the ratio A_0/A_1 with A_1 fixed at 100, 000.

as an effective technique in mobile molecular communication, where the distance between the two bio-nanomachines increases in proportion to the square root of time and the diffusion coefficients of Tx and Rx; changing time-related parameters (k and T) and the diffusion coefficients of Tx and Rx ($D_{\mathrm{T,R}}$) can thus lead to an increase in distance and reduce the achievable rate significantly. The numerical results also show that the reduction in achievable rate due to changes in these parameters can be compensated by increasing the number of measurements.

VI. CONCLUSION

We have developed mathematical models to describe mobile molecular communication where a mobile transmitter bio-nanomachine releases a pre-defined number of molecules and a mobile receiver bio-nanomachine extracts information by measuring the concentration of molecules on multiple occasions. In mobile molecular communication where transmitter and receiver bio-nanomachines move randomly, the distance between the two bio-nanomachines increases in proportion to the square root of time and diffusion coefficients of the two bio-nanomachines; this can decrease the achievable rate significantly. Numerical results using the models showed that multiple measurements serve as an effective means to compensate the reduction in achievable rate in mobile molecular communication.

In future work, we first design a more complex demodulation method using the molecule concentrations obtained from multiple measurements. In the present model, the receiver bio-nanomachine implements a simple demodulation method. It makes multiple measurements of the concentration of molecules, and receives '1' from when the concentration of molecules in any measurement exceeds a threshold, or '0' otherwise. This simple demodulation method can be easily implemented onto bio-nanomachines using concentration-dependent chemical reactions. Alternatively, more complex demodulation methods may be applicable to a receiver with computational capabilities (e.g., an electrical device [6], [7]). In such cases, a receiver may use the time-series data of molecule concentrations to more accurately determine information transmitted.

Future work also includes developing more realistic mobile molecular communication models. One possible extension is to consider stochastic interactions between the receiver bio-nanomachine and molecules while the receiver bio-nanomachine moves. The receiver's surface receptors bind to and unbind from molecules probabilistically [60]–[62] while the receiver bio-nanomachine performs random walks. It is also possible that the motion of bio-nanomachines produces a flow in the environment and such a flow in turn affects the diffusion of molecules. Future work is therefore to consider these dynamic and stochastic aspects of mobile molecular communication and develop more realistic models.

REFERENCES

[1] N. Farsad, H. B. Yilmaz, A. Eckford, C.-B. Chae, and W. Guo, "A comprehensive survey of recent advancements in molecular communication," *IEEE Commun. Surveys Tuts.*, vol. 18, no. 3, pp. 1887–1919, 3rd Quart., 2016.
[2] A. Gohari, M. Mirmohseni, and M. Nasiri-Kenari, "Information theory of molecular communication: Directions and challenges," *IEEE Trans. Mol. Biol. Multi-Scale Commun.*, vol. 2, no. 2, pp. 120–142, Dec. 2016.
[3] T. Nakano, "Molecular communication: A 10 year retrospective," *IEEE Trans. Mol. Biol. Multi-Scale Commun.*, vol. 3, no. 2, pp. 71–78, Jun. 2017.
[4] T. Nakano, A. Eckford, and T. Haraguchi, *Molecular Communication*. Cambridge, U.K.: Cambridge Univ. Press, 2013.
[5] Y. Okaie, T. Nakano, T. Hara, and S. Nishio, *Target Detection and Tracking By Bionanosensor Networks* (SpringerBriefs in Computer Science). Singapore: Springer, 2016.
[6] M. J. Moore and T. Nakano, "Multiplexing over molecular communication channels from nanomachines to a micro-scale sensor device," in *Proc. IEEE Global Commun. Conf. (GLOBECOM)*, Dec. 2012, pp. 4302–4307.
[7] M. J. Moore, Y. Okaie, and T. Nakano, "Diffusion-based multiple access by nano-transmitters to a micro-receiver," *IEEE Commun. Lett.*, vol. 18, no. 3, pp. 385–388, Mar. 2014.
[8] Y. Okaie and T. Nakano, "Binary concentration shift keying with multiple measurements of molecule concentration in mobile molecular communication," in *Bio-inspired Information and Communication Technologies*, vol. 329. Cham, Switzerland: Springer, 2020, pp. 42–51.
[9] H. C. Berg and E. M. Purcell, "Physics of chemoreception," *Biophys. J.*, vol. 20, no. 2, pp. 193–219, Nov. 1977.
[10] R. G. Endres and N. S. Wingreen, "Accuracy of direct gradient sensing by single cells," *Proc. Nat. Acad. Sci. USA*, vol. 105, no. 41, pp. 15749–15754, Oct. 2008.
[11] P. J. Thomas and A. W. Eckford, "Capacity of a simple intercellular signal transduction channel," *IEEE Trans. Inf. Theory*, vol. 62, no. 12, pp. 7358–7382, Dec. 2016.
[12] H. Nguyen, P. Dayan, and G. J. Goodhill, "How receptor diffusion influences gradient sensing," *J. Roy. Soc. Interface*, vol. 12, no. 102, Jan. 2015, Art. no. 20141097.
[13] C. West and A. C. Hanyaloglu, "Minireview: Spatial programming of G protein-coupled receptor activity: Decoding signaling in health and disease," *Mol. Endocrinol.*, vol. 29, no. 8, pp. 1095–1106, Aug. 2015.
[14] E. Shitiri, A. Vasilakos, and H.-S. Cho, "Biological oscillators in nanonetworks—Opportunities and challenges," *Sensors*, vol. 18, no. 5, p. 1544, May 2018.
[15] J.-L. Martiel and A. Goldbeter, "A model based on receptor desensitization for cyclic AMP signaling in dictyostelium cells," *Biophys. J.*, vol. 52, no. 5, pp. 807–828, Nov. 1987.
[16] M. De Pittà, V. Volman, H. Levine, and E. Ben-Jacob, "Multimodal encoding in a simplified model of intracellular calcium signaling," *Cognit. Process.*, vol. 10, no. S1, pp. 55–70, Feb. 2009.
[17] T. Nakano, Y. Okaie, S. Kobayashi, T. Hara, Y. Hiraoka, and T. Haraguchi, "Methods and applications of mobile molecular communication," *Proc. IEEE*, vol. 107, no. 7, pp. 1442–1456, Jul. 2019.

[18] B. Atakan and O. B. Akan, "An information theoretical approach for molecular communication," in *Proc. 2nd Bio-Inspired Models Netw., Inf. Comput. Syst. (Bionetics)*, Dec. 2007, pp. 33–40.
[19] M. U. Mahfuz, D. Makrakis, and H. T. Mouftah, "On the characterization of binary concentration-encoded molecular communication in nanonetworks," *Nano Commun. Netw.*, vol. 1, no. 4, pp. 289–300, Dec. 2010.
[20] H. B. Yilmaz, N.-R. Kim, and C.-B. Chae, "Effect of ISI mitigation on modulation techniques in molecular communication via diffusion," in *Proc. ACM 1st Annu. Int. Conf. Nanosc. Comput. Commun. (NANOCOM)*, 2007, pp. 1–9.
[21] T. Nakano, Y. Okaie, and J.-Q. Liu, "Channel model and capacity analysis of molecular communication with Brownian motion," *IEEE Commun. Lett.*, vol. 16, no. 6, pp. 797–800, Jun. 2012.
[22] A. Singhal, R. K. Mallik, and B. Lall, "Performance analysis of amplitude modulation schemes for diffusion-based molecular communication," *IEEE Trans. Wireless Commun.*, vol. 14, no. 10, pp. 5681–5691, Oct. 2015.
[23] N. Farsad, Y. Murin, A. Eckford, and A. Goldsmith, "On the capacity of diffusion-based molecular timing channels," in *Proc. IEEE Int. Symp. Inf. Theory (ISIT)*, Jul. 2016, pp. 1023–1027.
[24] N. Farsad, W. Guo, and A. W. Eckford, "Tabletop molecular communication: Text messages through chemical signals," *PLoS ONE*, vol. 8, no. 12, Dec. 2013, Art. no. e82935.
[25] A. O. Kislal, B. C. Akdeniz, C. Lee, A. E. Pusane, T. Tugcu, and C.-B. Chae, "ISI-mitigating channel codes for molecular communication via diffusion," *IEEE Access*, vol. 8, pp. 24588–24599, 2020.
[26] M. Damrath and P. A. Hoeher, "Low-complexity adaptive threshold detection for molecular communication," *IEEE Trans. Nanobiosci.*, vol. 15, no. 3, pp. 200–208, Apr. 2016.
[27] Z. Luo, L. Lin, and M. Ma, "Offset estimation for clock synchronization in mobile molecular communication system," in *Proc. IEEE Wireless Commun. Netw. Conf.*, Apr. 2016, pp. 1–6.
[28] L. Lin, Q. Wu, F. Liu, and H. Yan, "Mutual information and maximum achievable rate for mobile molecular communication systems," *IEEE Trans. Nanobiosci.*, vol. 17, no. 4, pp. 507–517, Oct. 2018.
[29] A. Ahmadzadeh, V. Jamali, and R. Schober, "Stochastic channel modeling for diffusive mobile molecular communication systems," *IEEE Trans. Commun.*, vol. 66, no. 12, pp. 6205–6220, Dec. 2018.
[30] S. Huang, L. Lin, H. Yan, J. Xu, and F. Liu, "Statistical analysis of received signal and error performance for mobile molecular communication," *IEEE Trans. Nanobiosci.*, vol. 18, no. 3, pp. 415–427, Jul. 2019.
[31] Z. Jia, X. Liao, and Z. Wu, "Signal detection for mobile molecular communication, based on concentration difference," in *Proc. Int. Conf. Artif. Intell. Adv. Manuf. (AIAM)*, 2019, pp. 1–5.
[32] C. Luo, X. Wu, L. Lin, C. Wang, and F. Liu, "Non-coherent signal detection technique for mobile molecular communication at high data rates," in *Proc. IEEE Global Commun. Conf. (GLOBECOM)*, Dec. 2019, pp. 1–6.
[33] S. Huang, L. Lin, W. Guo, H. Yan, J. Xu, and F. Liu, "Initial distance estimation and signal detection for diffusive mobile molecular communication," *IEEE Trans. Nanobiosci.*, vol. 19, no. 3, pp. 422–433, Jul. 2020.
[34] G. Chang, L. Lin, and H. Yan, "Adaptive detection and ISI mitigation for mobile molecular communication," *IEEE Trans. Nanobiosci.*, vol. 17, no. 1, pp. 21–35, Jan. 2018.
[35] X. Mu, H. Yan, B. Li, M. Liu, R. Zheng, Y. Li, and L. Lin, "Low-complexity adaptive signal detection for mobile molecular communication," *IEEE Trans. Nanobiosci.*, vol. 19, no. 2, pp. 237–248, Apr. 2020.
[36] L. Chouhan, P. K. Sharma, and N. Varshney, "Optimal transmitted molecules and decision threshold for drift-induced diffusive molecular channel with mobile nanomachines," *IEEE Trans. Nanobiosci.*, vol. 18, no. 4, pp. 651–660, Oct. 2019.
[37] L. Lin, Q. Wu, M. Ma, and H. Yan, "Concentration-based demodulation scheme for mobile receiver in molecular communication," *Nano Commun. Netw.*, vol. 20, pp. 11–19, Jun. 2019.
[38] T. Nakano, L. Lin, Y. Okaie, C. Wu, H. Yan, T. Hara, and K. Harumoto, "Random cell motion enhances the capacity of cell-cell communication," *IEEE Trans. Mol. Biol. Multi-Scale Commun.*, vol. 5, no. 2, pp. 158–162, Nov. 2019.
[39] N. Varshney, A. Patel, W. Haselmayr, A. K. Jagannatham, P. K. Varshney, and A. Nallanathan, "Impact of intermediate nanomachines in multiple cooperative nanomachine-assisted diffusion advection mobile molecular communication," *IEEE Trans. Commun.*, vol. 67, no. 7, pp. 4856–4871, Jul. 2019.
[40] L. Chouhan and P. K. Sharma, "Molecular communication in three-dimensional diffusive channel with mobile nanomachines," *Nano Commun. Netw.*, vol. 24, p. 32, Mar. 2020.
[41] L. Turner, W. S. Ryu, and H. C. Berg, "Real-time imaging of fluorescent flagellar filaments," *J. Bacteriol.*, vol. 182, no. 10, pp. 2793–2801, May 2000.
[42] N. Farsad, A. W. Eckford, S. Hiyama, and Y. Moritani, "A simple mathematical model for information rate of active transport molecular communication," in *Proc. IEEE Conf. Comput. Commun. Workshops (INFOCOM WKSHPS)*, Jun. 2011, pp. 473–478.
[43] A. Guney, B. Atakan, and O. B. Akan, "Mobile ad hoc nanonetworks with collision-based molecular communication," *IEEE Trans. Mobile Comput.*, vol. 11, no. 3, pp. 353–366, Mar. 2012.
[44] J. Namba, T. Nakano, Y. Okaie, and T. Hara, "Epidemic information dissemination for molecular communication among mobile bio-nanomachines," in *Proc. 3rd ACM Int. Conf. Nanosc. Comput. Commun. (NANOCOM)*, Sep. 2016, pp. 1–2.
[45] S. Ishiyama, T. Nakano, Y. Okaie, and T. Hara, "Epidemic information dissemination in mobile molecular communication systems," in *Proc. IEEE Global Commun. Conf. (GLOBECOM)*, Dec. 2018, pp. 1–7.
[46] P. He, B. Pi, and Q. Liu, "Calcium signaling in mobile molecular communication networks: From a multimedia view," *IEEE Access*, vol. 7, pp. 164825–164834, 2019.
[47] N. Rady Raz, M.-R. Akbarzadeh-T., and M. Tafaghodi, "Bioinspired nanonetworks for targeted cancer drug delivery," *IEEE Trans. Nanobiosci.*, vol. 14, no. 8, pp. 894–906, Dec. 2015.
[48] T. Nakano, Y. Okaie, S. Kobayashi, T. Koujin, C.-H. Chan, Y.-H. Hsu, T. Obuchi, T. Hara, Y. Hiraoka, and T. Haraguchi, "Performance evaluation of Leader–Follower-Based mobile molecular communication networks for target detection applications," *IEEE Trans. Commun.*, vol. 65, no. 2, pp. 663–676, Feb. 2017.
[49] Y. Okaie, S. Ishiyama, and T. Hara, "Leader-follower-amplifier based mobile molecular communication systems for cooperative drug delivery," in *Proc. IEEE Global Commun. Conf.*, Dec. 2018, pp. 206–212.
[50] L. Canzian, K. Zhao, G. C. L. Wong, and M. van der Schaar, "A dynamic network formation model for understanding bacterial self-organization into micro-colonies," *IEEE Trans. Mol. Biol. Multi-Scale Commun.*, vol. 1, no. 1, pp. 76–89, Mar. 2015.
[51] T. Nakano and T. Suda, "Modeling and simulations of bio-nanomachines for spatiotemporal pattern formation," in *Proc. 5th ACM Int. Conf. Nanosc. Comput. Commun. (NANOCOM)*, Sep. 2018, pp. 1–6.
[52] Y. Okaie, "Cluster formation by mobile molecular communication systems," *IEEE Trans. Mol. Biol. Multi-Scale Commun.*, vol. 5, no. 2, pp. 153–157, Nov. 2019.
[53] N. Islam, S. Pal, S. Balasubramaniam, and S. Misra, "Energy-aware tracking of mobile targets by bacterial nanonetworks," *IEEE Trans. Mobile Comput.*, early access, Apr. 23, 2020, doi: 10.1109/TMC.2020.2990134.
[54] D. Kilinc and O. B. Akan, "Receiver design for molecular communication," *IEEE J. Sel. Areas Commun.*, vol. 31, no. 12, pp. 705–714, Dec. 2013.
[55] H. C. Berg, *Random Walks in Biology, New, Expanded Edition*. Princeton, NJ, USA: Princeton Univ. Press, 1993.
[56] K. Schulten and I. Kosztin, *Lectures Theoretical Biophysics*. Champaign, IL, USA: Univ. Illinois Urbana-Champaign, 2000.
[57] J. Crank, *The Mathematics of Diffusion*. London, U.K.: Oxford Science, 1986.
[58] A. Ahmadzadeh, V. Jamali, A. Noel, and R. Schober, "Diffusive mobile molecular communications over time-variant channels," *IEEE Commun. Lett.*, vol. 21, no. 6, pp. 1265–1268, Jun. 2017.
[59] S. Huang, L. Lin, H. Yan, J. Xu, and F. Liu, "Mean and variance of received signal in diffusion-based mobile molecular communication," in *Proc. IEEE Global Commun. Conf. (GLOBECOM)*, Dec. 2018, pp. 1–6.
[60] H. B. Yilmaz, A. C. Heren, T. Tugcu, and C.-B. Chae, "Three-dimensional channel characteristics for molecular communications with an absorbing receiver," *IEEE Commun. Lett.*, vol. 18, no. 6, pp. 929–932, Jun. 2014.
[61] A. Akkaya, H. Birkan Yilmaz, C.-B. Chae, and T. Tugcu, "Effect of receptor density and size on signal reception in molecular communication via diffusion with an absorbing receiver," 2014, *arXiv:1411.6372*. [Online]. Available: http://arxiv.org/abs/1411.6372
[62] M. Femminella, G. Reali, and A. V. Vasilakos, "A molecular communications model for drug delivery," *IEEE Trans. Nanobiosci.*, vol. 14, no. 8, pp. 935–945, Dec. 2015.